



## In situ observed relationships between skin temperatures and 2 m air temperatures in the Arctic

Pia Nielsen-Englyst<sup>1</sup>, Jacob L. Høyer<sup>1</sup>, Kristine S. Madsen<sup>1</sup>, Gorm Dybkjær<sup>1</sup>, Rasmus Tonboe<sup>1</sup>, Emy Alerskans<sup>1</sup>

5 <sup>1</sup>Danish Meteorological Institute, DK-2100 Copenhagen Ø, Denmark

*Correspondence to:* Pia Nielsen-Englyst (pne@dmi.dk)

### Abstract.

To facilitate the combined use of traditional 2 m air temperature (T2m) observations from weather stations in the Arctic and skin temperature (Tskin) observations from satellites the relationship between high latitude snow and ice Tskin and T2m is  
10 quantified. Multiyear data records of simultaneous Tskin and T2m from 20 different in situ sites have been analysed, covering the Greenland Ice Sheet (GrIS), sea ice in the Arctic Ocean, and coastal snow covered land in North Alaska. The diurnal and seasonal temperature variabilities and the impacts from clouds and wind on the T2m-Tskin differences are quantified. Considering all stations, T2m is on average 1.37°C warmer than Tskin, with the largest differences at the GrIS stations (mean of diff. of 1.64°C). Tskin and T2m are often highly correlated, and the two temperatures are almost identical  
15 (<0.5°C) at particularly times of the day and year, and during certain conditions. The data analysed here indicate the best agreement between Tskin and T2m around noon and early afternoon during spring and fall. However, Tskin is often colder than T2m by 2°C or more, with the largest differences occurring during winter, when it is dark and during night. This is seen for all observation sites, where a negative surface radiation balance makes the surface colder than the atmosphere, resulting in a surface-driven surface air temperature inversion. The observation sites on sea ice and in Alaska show that the surface-  
20 based inversion decreases as a function of wind speed, because of turbulent mixing. The sites on the GrIS show an interesting feature, with the maximum inversion occurring not at calm winds, but at wind speeds of about 5 m s<sup>-1</sup>, likely due to the katabatic winds, which are most prominent at this wind speed. Clouds tend to reduce the vertical temperature gradient, by warming the surface, resulting in a mean T2m-Tskin difference of 0.53°C considering all stations. Following that the influence of clouds on Tskin has been assessed by comparing clear-sky Tskin observations with all-sky observations  
25 averaged for the time windows of: 24 h, 72 h and 1 month. The largest clear-sky biases are generally found when 1 month averages are used and smallest for 24 h. The mean clear-sky bias for the 24 h average is -0.28°C, ranging from -0.10°C in summer to -0.95°C in winter. The expected clear-sky biases and the difference between Tskin and T2m are of practical value for researchers and operational users that aim at integrating satellite observations with ocean, sea-ice or atmospheric models.



## 1 Introduction

The Arctic region is warming about twice as much as the global average because of Arctic amplification (Graversen et al., 2008). Greenland meteorological data show that the last decade (2000s) is the warmest since meteorological measurements of surface air temperatures started in the 1780s (Cappelen, 2016; Masson-Delmotte et al., 2012) and the period 1996-2014 yields an above average warming trend compared to the past six decades (Abermann et al., 2017). The reason for the Arctic amplification is a number of positive feedback mechanisms i.e. the ice-albedo feedback which is driven by the retreat of Arctic sea ice, terrestrial snow cover, and a darkening of the Greenland Ice Sheet (GrIS). The atmospheric warming and decreasing albedo of the ice sheet have resulted in an accelerated mass loss of the GrIS over the past decade (Box et al., 2012). Future projections of the GrIS mass balance show that the surface melt is exponentially increasing as a function of the surface air temperature (Franco et al., 2013). Further, the Arctic warming contributes to mid latitude weather events (Cohen et al., 2014; Screen and Simmonds, 2010; Serreze and Francis, 2006). It is therefore important to monitor the temperature of the Arctic to understand and predict the local as well as global effects of climate change. Current global surface temperature products traditionally include Arctic near surface air temperatures from buoys and automatic weather stations (AWSs) (Hansen et al., 2010; Jones et al., 2012; Rayner, 2003). However, in situ observations are not available everywhere and the time series have gaps or limited duration. In particular, the Arctic ice regions are covered sparsely with in situ measurements, due to the extreme weather conditions and low population density (Reeves Eyre and Zeng, 2017). The global surface temperature products are thus based on a limited number of observations in this very important region. This means that crucial climatic signals and trends could be missed by poor coverage of the observational system.

A way to improve the spatial and temporal data coverage of the surface temperature is by the use of satellite remote sensing. However, current global surface temperature products estimate the 2 m air temperature (T2m; Hansen et al., 2010; Jones et al., 2012), whereas the variable retrieved from satellite observations is the surface skin temperature (Tskin). A surface-based air temperature inversion is a common feature of the Arctic winter (Serreze et al., 1992; Zhang et al., 2011). The inversion exists because of the imbalance between outgoing longwave radiation and incoming solar radiation, leading to a cooling of the surface, especially when the absorbed incoming solar radiation is small (during winter and night). An analysis based on observations from the Antarctic Plateau showed that the inversion continues all the way to the surface with the largest gradient between the surface and 20 cm above it (Hudson and Brandt, 2005). The surface-driven temperature inversion causes a difference between the T2m and the actual skin temperature at the snow/air interface. Previously, work has been done to characterize the relationship between the T2m and land surface temperatures observed from satellites and identified land cover, vegetation fraction and elevation as the dominating factors (Good et al., 2017). Few studies have investigated the temperature inversion in the ice regions for the lowest 2 m of the atmosphere focusing on limited time periods and single locations e.g. Summit, Greenland (Adolph et al., 2017; Hall et al., 2008), the South Pole (Hudson and Brandt, 2005) and the Arctic sea ice (Vihma and Pirazzini, 2005). Until now, no systematic studies have yet been made for the high latitude ice sheets and over sea ice.



The difference between the T2m and Tskin is very important in validation studies of remotely sensed temperatures. Several studies have used T2m observations for validating satellite Tskin products on the GrIS (Dybkjær et al., 2012; Hall et al., 2008; Koenig and Hall, 2010; Pérez Díaz et al., 2015; Shuman et al., 2014) and over the Arctic sea ice (Dybkjær et al., 2012) and found that a significant part of the differences could be attributed to the difference between the Tskin and T2m. Conversely, Rasmussen et al. (2018) used satellite Tskin observations in a simple way to correct the T2m in a coupled ocean and sea ice model and obtained an improved snow cover.

In order to facilitate the integrated use of Tskin and T2m from in situ observations, satellite observations and models, there is thus a need for a better understanding and characterization of the observed relationship. The aim of this paper is to bring further insight into this relationship, using in situ observations. This study extends the previous analyses to include multiyear observational records from 20 different sites located at the GrIS, Arctic sea ice, and the coastal region of North Alaska. The aim is to identify the key parameters influencing the temperature difference between the surface and 2 m height and to assess under which conditions Tskin is, or is not, a good proxy for the T2m and to quantify the differences, using Tskin as a proxy for T2m. The findings are intended to aid the users of satellite data and to support estimation of T2m using satellite Tskin observations. In the response to the latter, an effort has also been made to estimate a clear-sky bias of Tskin based on in situ observations. The paper is structured such that Sect. 2 describes the in situ data. Section 3 gives an introduction to the near surface boundary conditions. The results are presented in Sect. 4 and discussed in Sect. 5. Conclusions are given in Sect. 6.

## 2 Data

In situ observations have been collected from various sources and campaigns covering ice and snow surfaces to assemble the Danish Meteorological Institute (DMI) database used in this study. The focus has been on collecting in situ data with simultaneous observations of Tskin, measured with a radiometer, and T2m, measured with a shielded and ventilated thermometer about 2 m above the surface, in the Arctic. Further details are provided for each data source in Sect. 2.1-2.6.

### 2.1 PROMICE

Data have been obtained from the Programme for Monitoring of the Greenland Ice Sheet (PROMICE) provided by the Geological Survey of Denmark and Greenland (GEUS). PROMICE was initiated in 2007 by the Danish Ministry of Climate and Energy, and operated by GEUS in collaboration with the National Space Institute at the Technical University of Denmark and Asiaq (Greenland Survey; e.g. Ahlstrøm et al., 2008). PROMICE collects in situ observations from a number of AWSs along the margin of the GrIS (Fig. 2). Each observational site has one or more stations; typically one located in the ablation zone and another located near the equilibrium line altitude. Only the high-altitude sites (elevation > 500 m) have been used in this study in order to ensure year-round snow cover. PROMICE Tskin has been calculated from up-welling longwave radiation assuming blackbody radiation properties for snow and ice. The air temperature is measured by a thermometer at a



height of 2.7 m, while the wind speed is measured at about 3.1 m height, if no snow is present. Snow accumulation during winter reduces the measurement height. In this study, we use hourly averages of the data, provided by PROMICE.

## 2.2 ARM

The Atmospheric Radiation Measurement (ARM) Program (Ackerman and Stokes, 2003; Stamnes et al., 1999) was established in 1989 and it provides data on the cloud and radiative processes at high latitudes. Three ARM sites from the North Slope of Alaska (NSA) are used in this study: Atkasuk (ATQ), Barrows (BAR), and Oliktok Point (OLI). The stations provide surface snow infrared (IR) temperature measured using a Heitronics KT19.85 IR Radiation Pyrometer (Moris, 2006) and air temperature measured at 2 m height. Wind speed is measured at 10 m height. The ARM stations have seasonal snow coverage, i.e. the snow melts away in summer. Data where the surface albedo is less than 0.30 indicate that the snow has disappeared and these have been excluded to ensure that we only consider snow/ice covered surfaces.

## 2.3 ICEARC

We use the ICEARC sea ice temperature and radiation data set from DMI field campaign in Qaanaaq. The DMI AWS is deployed on first-year sea ice in Qaanaaq and is funded by the European climate research project, ICE-ARC. The AWS was deployed for the first time in late January 2015 at the north side of the fjord Inglefield Bredning and recovered in early June before break-up of the fjord ice. The campaign has been repeated every year since then and the data used in this study is procured by fieldwork done in the periods Jan.-Jun., 2015-2017. The AWS is equipped to measure snow surface IR temperature and air temperature at 1 and 2 m heights. In this study, the 1 m air temperature is used instead of the 1-2 m air temperature, as the differences  $T_{skin}$  vs. 1 m temperature resembled the other stations significantly better than the  $T_{skin}$  vs. 2 temperature at this site, during winter and spring. The data used here are 10 minute snapshots (Høyer et al., 2017) and are referenced as: DMI\_Q in this paper.

## 2.4 SHEBA

The Surface Heat Budget of the Arctic (SHEBA) experiment is a multiagency program led by the National Science Foundation and the Office of Naval Research. The data used in this study originates from deployment of a Canadian icebreaker, DesGroseilliers, in the Arctic ice pack 570 km northeast of Prudhoe Bay, Alaska in 1997 (Uttal et al., 2002). During its year-long deployment, SHEBA provided atmospheric and sea ice measurements from the icebreaker and the surrounding frozen ice floe. The data used here contain hourly averaged data collected by the SHEBA Atmospheric Surface Flux Group (ASFG) and Dr. J. Liljegren from the ARM project. The SHEBA ASFG installed a 20 m tall tower, which was used to obtain measurements of the surface energy budget, focusing on the turbulent heat fluxes and the near surface boundary layer structure (Bretherton et al., 2000; Persson, 2002). Five different levels, varying in height from 2.2-18.2 m, had mounted a temperature/humidity probe and a sonic anemometer. We use air temperature and wind data from the lowest mounted instruments (2.2 m), which vary in height from 1.9 to 3 m depending on snow accumulation and snow melt.



Three surface temperature measurements were measured from a General Eastern thermometer, an Eppley radiometer and a Barnes radiometer, available from April to September 2007. The Eppley is the most reliable, though there are periods when the other two are also reasonable, and one period (May), when the Eppley data may be slightly off. We use the best estimate of Tskin, which is based on slight corrections to the Eppley temperatures and the Barnes temperatures when Eppley was known to be wrong (Persson, 2002).

## 2.5 FRAM2014/15

The scientific program of the FRAM2014/15 expedition is carried out by the Nansen Center (NERSC) in co-operation with Alfred Wegener Institute, Helmholtz Centre for Polar and Marine Research, Germany, University of Bergen, Bjerknes Center for Climate Research and Norwegian Meteorological Institute. FRAM2014/15 is a Norwegian ice drift station deployed near the North Pole in August 2014 using a medium-sized hovercraft as logistic and scientific platform (Kristoffersen and Hall, 2014). This type of mission allows exploration of the Arctic Ocean not accessible to icebreakers, and enables scientific field experiments, which require physical presence. The hovercraft was operated by two people and by the end of March 2015 they had drifted 1.450 km. During the drift with sea ice they obtained Tskin measurements by Cambell Scientific IR120 (later corrected for sky temperature and emissivity) and 100 profiles of air temperature.

## 2.6 TARA

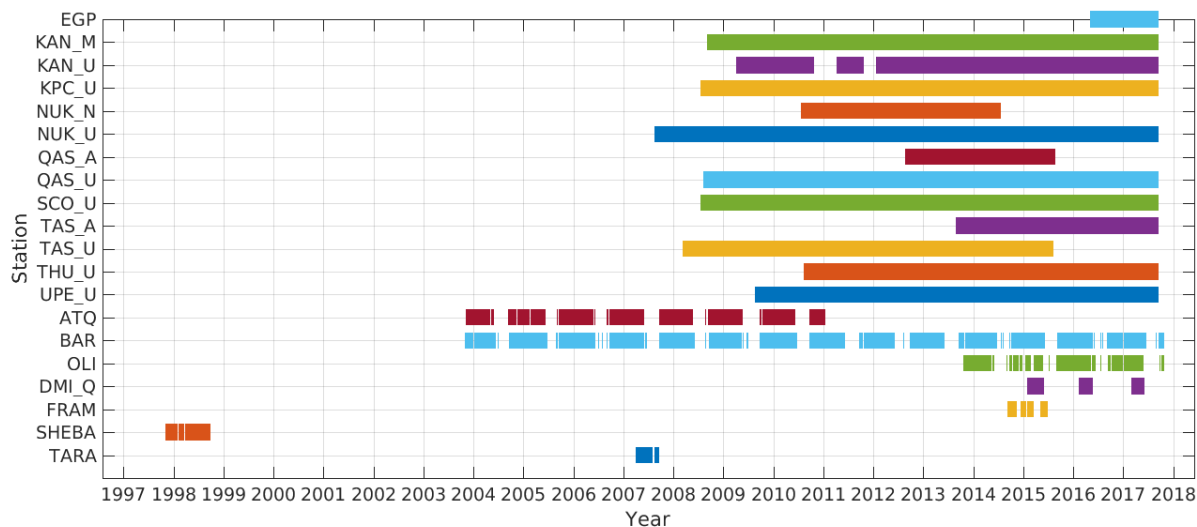
The Tara multidisciplinary experiment was a part of the international polar year DAMOCLES (Developing Arctic Modelling and Observing Capabilities for Long-term Environmental Studies) program (Gascard et al., 2008; Vihma et al., 2008). The experiment took place from late August 2006 and the ship drifted for fifteen months frozen into the sea ice in the transpolar drift through the Arctic Ocean. Air temperature and wind speed were measured from a 10 m tall Aanderaa weather mast at the heights of 1, 2, 5, and 10 m and wind direction was measured at 10 m height. We use the air temperatures and wind speed measured at 2 m height. They also had an Eppley broadband radiation mast with two sensors for longwave fluxes and two sensors for shortwave fluxes (upward and downward looking). The downward looking IR sensor also provides Tskin from April to September 2007. The data used in this study are 10 minute averages.

Table 1 gives an overview of the data and the abbreviations used in this paper. Figure 1 shows the temporal data coverage, while the geographical distribution and elevations are shown in Fig. 2. Observations from the sites in Table 1 include T2m, Tskin, wind speed, shortwave- and longwave radiations. Measurement heights vary depending on the site and snow depth, but for this paper near-surface air temperatures are referred to as 2 m air temperature despite these variations. All data has been screened for spikes and other data artefacts using both automated and visual quality checks.



**Table 1 Observation sites used in this study.**

Project	Site	Station	Surface	Latitude (°N)	Longitude (°W)	Elevation (m)	Start date	End date
PROMICE	East Grip	EGP	Land ice	75.62	35.97	2660	01/05/2016	15/09/2017
PROMICE	Kangerlussuaq	KAN_M	Land ice	67.07	48.84	1270	02/09/2008	16/09/2017
PROMICE	Kangerlussuaq	KAN_U	Land ice	67.00	47.03	1840	04/04/2009	16/09/2017
PROMICE	Crown Prince Christian Land	KPC_U	Land ice	79.83	25.17	870	17/07/2008	16/09/2017
PROMICE	Nuuk	NUK_N	Land ice	64.95	49.89	920	25/07/2010	25/07/2014
PROMICE	Nuuk	NUK_U	Land ice	64.51	49.27	1120	20/08/2007	16/09/2017
PROMICE	Qassimiut	QAS_A	Land ice	61.24	46.73	1000	20/08/2012	24/08/2015
PROMICE	Qassimiut	QAS_U	Land ice	61.18	46.82	900	07/08/2008	16/09/2017
PROMICE	Scoresbysund	SCO_U	Land ice	72.39	27.23	970	21/07/2008	16/09/2017
PROMICE	Tasiilaq	TAS_A	Land ice	65.78	38.90	890	28/08/2013	16/09/2017
PROMICE	Tasiilaq	TAS_U	Land ice	65.67	38.87	570	15/08/2007	13/08/2015
PROMICE	Thule	THU_U	Land ice	76.42	68.15	760	09/08/2010	16/09/2017
PROMICE	Upernavik	UPE_U	Land ice	72.89	53.58	940	17/08/2009	16/09/2017
ARM	Atqasuk	ATQ	Land ice	70.47	149.89	2	07/11/2003	17/01/2011
ARM	Barrows	BAR	Land ice	71.32	156.62	8	31/10/2003	26/10/2017
ARM	Oliktok Point	OLI	Land ice	70.50	157.41	20	18/10/2013	26/10/2017
ICEARC	Qaanaaq	DMI_Q	Sea ice	77.43	69.14	Sea level	31/01/2015	08/06/2017
FRAM2014/15	Arctic Ocean	FRAM	Sea ice	82.22-89.35	-180.00-180.00	Sea level	05/09/2014	3/07/2015
SHEBA	Arctic Ocean	SHEBA	Sea ice	74.62-80.37	143.92-168.15	Sea level	01/11/1997	26/09/1998
TARA	Arctic Ocean	TARA	Sea ice	71.41-88.54	0.01-148.28	Sea level	01/04/2007	20/09/2007



**Figure 1: Temporal coverage for each data site included in this study.**

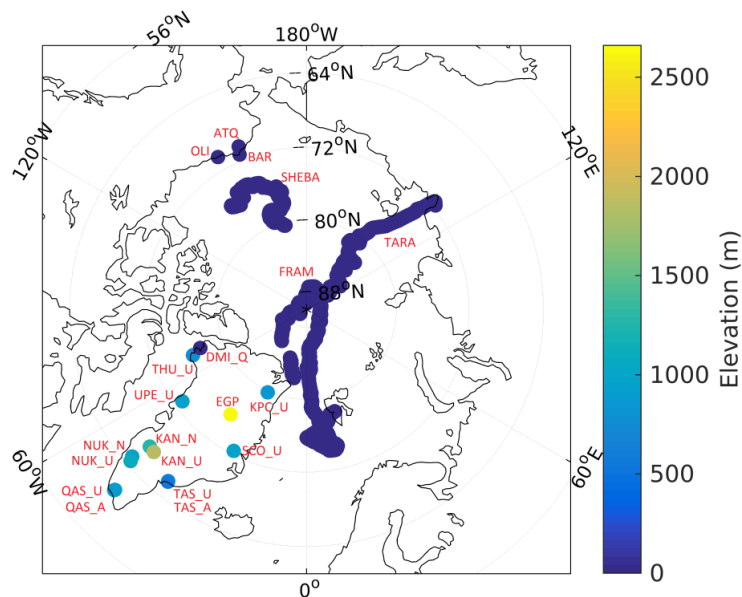


**Figure 2: Spatial coverage and elevation for each site included in this study. The colour bar is elevation in meters.**

5

## 2.7 Radiometric observations of Tskin

The Tskin observations used in this study are all derived from radiometric observations, but with spectral characteristics that range from the Heitronics KT19.85 with a spectral response function from 9.5-11.5  $\mu\text{m}$  over Cambell Scientific IR 120 with



a 8-14  $\mu\text{m}$  spectral window to broadband longwave observations from  $\sim$ 4-40  $\mu\text{m}$ . The emissivity of the ice surface varies for the different spectral windows and this leads to a difference in actual observed  $T_{\text{skin}}$  as the reflected sky temperature tends to be much colder than the ice surface. The contribution from the reflected cold sky is thus included in the radiometric observations but the ice and snow surfaces have generally very high emissivities, which reduce the sky effects (e.g. Dozier and Warren, 1982). In Høyer et al. (2017), the difference in emissivity between the KT15.85 and the IR120 was modelled using an IR snow and ice emissivity model with the spectral response functions for the two types of instruments. This resulted in averaged emissivities of 0.998 for the KT15.85 and 0.996 for the IR120 spectral windows for a typical snow surface and an incidence angle of 25 degrees. Using the same type of model for a broadband 4-40  $\mu\text{m}$  spectrum resulted in an emissivity of 0.997. The high emissivities for all three instruments mean that the contributions from the sky are small. For realistic conditions in the Arctic, this e.g. introduces an average difference of 0.06°C between the IR120 and the KT15.85 radiometer (which has a similar spectral response function as the KT19.85), with the IR120 being colder than the KT15.85 (Høyer et al., 2017).

Several of the stations (ATQ, BAR, OLI, DMI\_Q, SHEBA and FRAM) used here observed both narrow band and wide band IR observations of the ice surface. The two types of  $T_{\text{skin}}$  have been calculated and compared for each of the stations. A good agreement was observed with a mean difference between the two  $T_{\text{skin}}$  types of 0.034°C. In the following we use the narrow band  $T_{\text{skin}}$  observations when available and the broadband at the other stations and assume that all the  $T_{\text{skin}}$  derived observations have same characteristics.

## 2.8 Cloud cover

For all sites, the cloud cover fraction (CCF) has been estimated based on the relationship between T2m and down-welling longwave radiation ( $LW_d$ ), following the cloud cover estimation already included in the PROMICE data sets (van As, 2011; van As et al., 2005). It is based on Swinbank (1963), who presented a very simple approach for estimation of clear-sky (CCF=0) atmospheric longwave radiation as a function of T2m:

$$LW_{d_{clear}} = 9.365 \cdot 10^{-6} \cdot T2m^2 \cdot \sigma \cdot T2m^4, \quad (1)$$

where  $\sigma$  is Stefan-Boltzmann's constant. Overcast conditions (CCF=1) are assumed to occur when the observed  $LW_d$  exceeds the blackbody radiation emitted from the surface, which is calculated using T2m. The CCF for any observed T2m and  $LW_d$  pair is calculated by linear interpolation of the observed  $LW_d$ , between these theoretical clear-sky and overcast estimates (van As, 2011).

## 3. Introduction to the near surface boundary conditions

To perform an analysis of the  $T_{\text{skin}}$  and T2m relationship and interpret the results it is important to consider the surface energy balance and the specific characteristics that apply in the Arctic. The surface temperature and surface melt are driven



by the surface energy balance. The net surface energy balance is defined by the fluxes of energy between the atmosphere, the snow/ice surface and the underlying land, snow/ice, or ocean. The surface energy balance can be written

$$SW_d - SW_u + LW_d - LW_u + SH + LH + G = M,$$

where  $M$  is the net energy flux at the surface and  $SW_d$ ,  $SW_u$ ,  $LW_d$ ,  $LW_u$ ,  $SH$ ,  $LH$ , and  $G$  represent the down- and upwelling shortwave radiation, down- and upwelling longwave radiation, sensible and latent heat flux, and subsurface conductive energy, respectively. The energy fluxes have the unit  $\text{W m}^{-2}$ . All fluxes are defined as positive when adding energy to the surface. The net energy flux can be positive or negative. When it is negative the snow/ice will cool or liquid water will refreeze. Positive net energy flux is used for warming the surface or melting snow and ice at the surface, when the fluxes on the left cannot be balanced i.e. when the surface temperature is limited to the melting point.

The radiative budget of the polar regions is dominated by longwave radiation during much of the year and even during summer the shortwave radiation input is in the same order of magnitude as the incoming longwave radiation flux because of extensive cloud cover especially during late summer and the high surface albedo of the snow (Maykut, 1986).  $SW_d$  is the dominating source for ice melt in Greenland (van den Broeke et al., 2008; Box et al., 2012; van As et al., 2012), even though non-radiative energy fluxes can dominate during shorter periods (Fausto et al., 2016). On average, the non-radiative fluxes are an order of magnitude smaller than the radiation fluxes. However, because the net radiation balance is small compared to the large incoming and outgoing radiation fluxes then variations in  $SH$  and  $LH$  fluxes are anyway important for the total surface energy balance, the surface temperature, sea ice growth and melt processes. Surface winds interact strongly with the surface energy fluxes as the turbulent mixing increases as a function of wind speed (van As et al., 2005).

During winter and clear-skies when  $SW_d$  is negligible  $LW_u$  is higher than the  $LW_d$  at the surface because the atmosphere above the atmospheric boundary layer is colder than the surface and because the atmosphere is very dry (Maykut, 1986). When the heat conduction flux from below is limited on thick sea ice and on continental ice sheets the negative radiation budget at the surface makes the surface temperature colder than the surface air temperature, resulting in a surface-based temperature inversion. At low to moderate wind-speeds, where turbulent mixing is limited, this creates a very stable stratification of the lower atmosphere. On a sloping surface, the surface air starts to flow downslope, driven by the existence of a horizontal temperature gradient and gravity, crossing the contour lines at an angle of about  $45^\circ$  to the right (in the northern hemisphere) by the Coriolis force. The generated winds are called inversion/katabatic winds depending on the slope (Lettau and W. Schwerdtfeger, 1967). In the case of PROMICE sites on GrIS we will refer to these winds as katabatic winds. Both inversion winds and katabatic winds are characterised by stronger winds at more negative surface net radiation and a strong correlation between slope and wind direction.

Clouds play a complex role in the Arctic surface energy budget, both reflecting  $SW_d$  leading to a cloud shortwave cooling effect, and absorbing  $LW_u$  and emitting  $LW_d$ , which tend to have a warming effect. In the Arctic clouds have a predominantly warming effect on the surface (Intrieri, 2002; Walsh and Chapman, 1998) as the dry background atmosphere, more transparent to  $LW$  radiation, enhances the cloud longwave warming effect, while the high surface albedo and the high solar



zenith angles act to reduce the cloud shortwave cooling effect (Curry et al., 1996; Curry and Herman, 1985; Zygmuntowska et al., 2012).

## 4 Results

### 4.1 Diurnal and seasonal temperature variability

5 The local air and surface temperature conditions in the Arctic are to a large extent influenced by the length of the day or night in the Arctic, with extreme variations depending on latitude and time of the year. The temperature variability has several important temporal scales. In this study we will focus on the diurnal and seasonal temperature variations. As an example of the large seasonal variations, Fig. 3 shows the 2014 monthly mean diurnal temperature variation of Tskin and T2m at the upper PROMICE site in Kangerlussuaq, KAN\_U, during January, April, July and October. Considering all months, there is high correlation between Tskin and T2m ranging from 0.957 in April to 0.995 in October at KAN\_U. Both Tskin and T2m reach a maximum in July, while the coldest month is December (not shown). During winter and polar night, there is no clear diurnal cycle in neither T2m or Tskin, and T2m is higher than Tskin. However, during spring there is a strong diurnal cycle, with maximum temperatures coinciding with maximum daily insolation. At night, Tskin is colder than T2m, while the T2m-Tskin difference is small during daytime. The shadings indicate the standard deviations in T2m and Tskin, respectively. The largest variability is found in spring and winter.

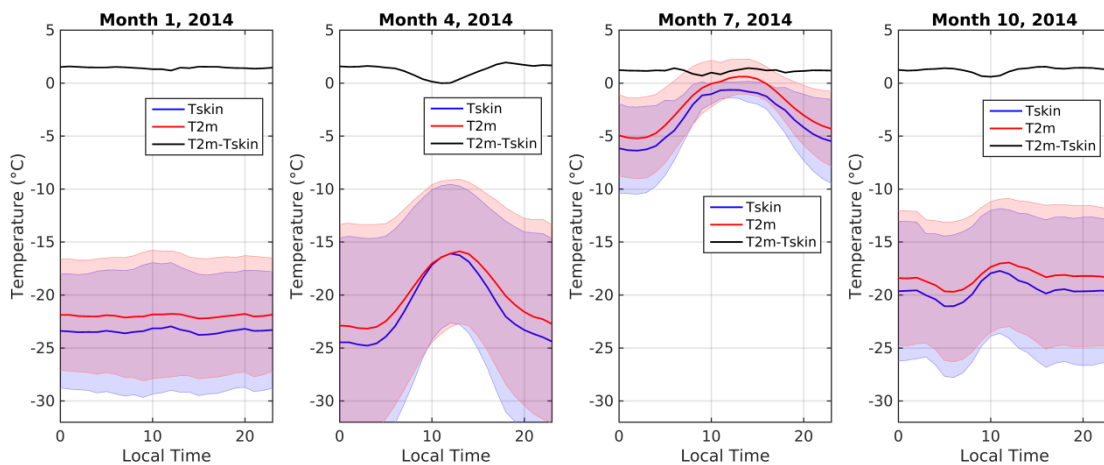


**Figure 3: Monthly diurnal variability of 2 m air temperature (red) and skin temperature (blue) at KAN\_U during the months: January, April, July and October. The black curves are the difference between the red and blue curves. The shadings indicate the standard deviations.**

20 The large seasonal variations in Fig. 3 and the relationship between T2m and Tskin are typical for all sites. Figure 4 shows the monthly mean Tskin for all sites and all years. EGP is by far the coldest site included in this analysis, with a monthly mean Tskin of  $-42^{\circ}\text{C}$  in January and a maximum of  $-11^{\circ}\text{C}$  in July. All sites reach a maximum in Tskin in July, regardless of



latitude. July is also the month with least variation in temperature among sites, while the winter months show a larger variance in Tskin among sites. The AWS data from the GrIS show the effect of altitude and latitude on Tskin, with the high altitude sites being the coldest (EGP, KAN\_U and KAN\_M) together with the most northern sites (THU\_U and KPC\_U). The southern and low altitude sites occur to be the warmest (e.g. TAS\_U, TAS\_A and SCO\_U). The sites on sea ice are comparable with the coldest sites on the GrIS (except from EGP), but are slightly warmer in summer.

Figure 5 shows the mean daily range (daily max – daily min difference) of Tskin as a function of month for all sites and all years. Again, the observations show a similar pattern across the diverse geographical locations. The mean daily range of all sites is 7.1°C during winter (Dec.-Feb.), 8.4°C in spring (Mar.-May), 3.3°C in summer (Jun.-Aug.), and 6.7°C in autumn (Sep.-Nov.). During summer the high elevation sites tend to have the largest daily range in Tskin, while the observations from sea ice show the smallest daily range. This is probably an effect of the warmer temperatures and the Tskin upper temperature limit at 0°C, the melting point for ice. This constraint is often seen for the sea ice data records during summer.

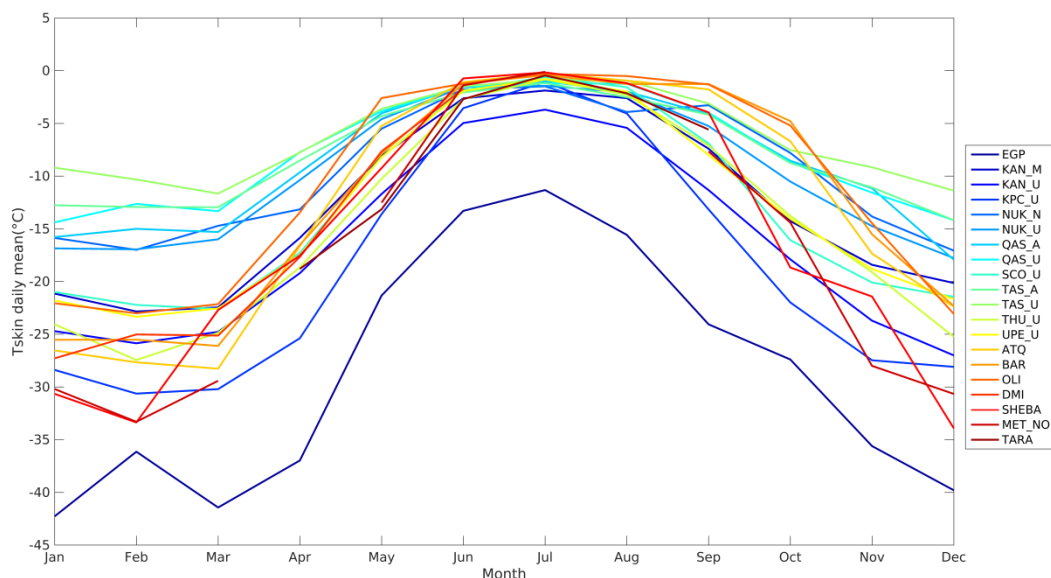


**Figure 4: Monthly mean skin temperature for all sites. See Table 1 for station location and type.**

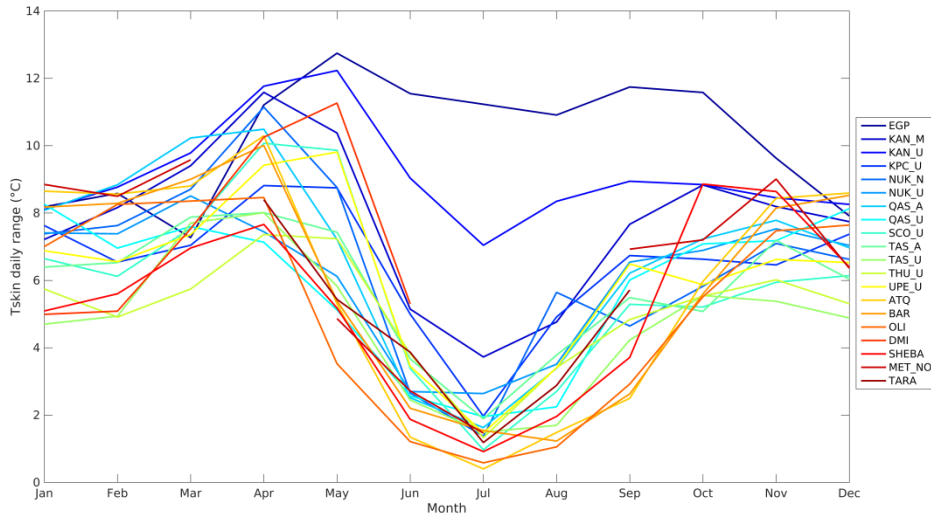


**Figure 5: Daily range of skin temperature as a function of month for all sites. See Table 1 for station location and type.**

Focusing on the relationship between T2m and Tskin, it is clear that even though Fig. 3 showed that the two temperatures have high correlation, it also showed that the T2m-Tskin difference is not constant throughout the day and year (at KAN\_U). The mean difference between T2m and Tskin for all observation sites, weighted equal, as a function of time of year, is shown in Fig. 6. On average the monthly mean T2m is 1.44°C warmer than monthly mean Tskin with the largest differences in July and August. The figure also shows the monthly mean standard deviation of the T2m-Tskin difference. The largest variability of the difference is found in Mar.-May, while the summer months have least variability in the T2m-Tskin difference.

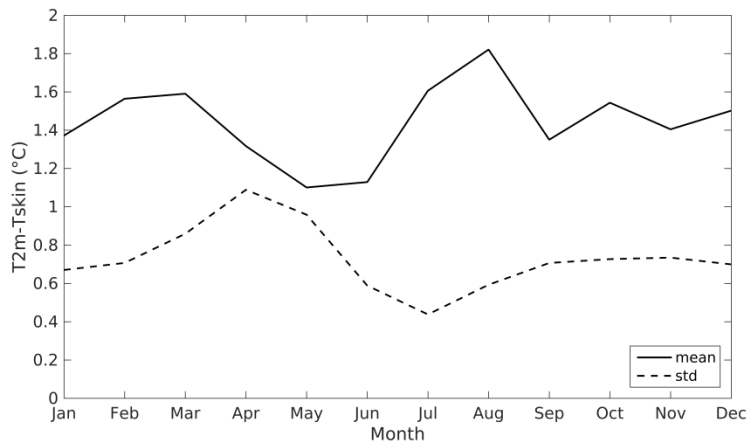


**Figure 6: Monthly mean difference in 2 m air temperature and skin temperature (T2m-Tskin) for all data sites with time coverage as listed in Table 1 (solid line). The dashed line shows the mean of the standard deviations from the different observation sites.**

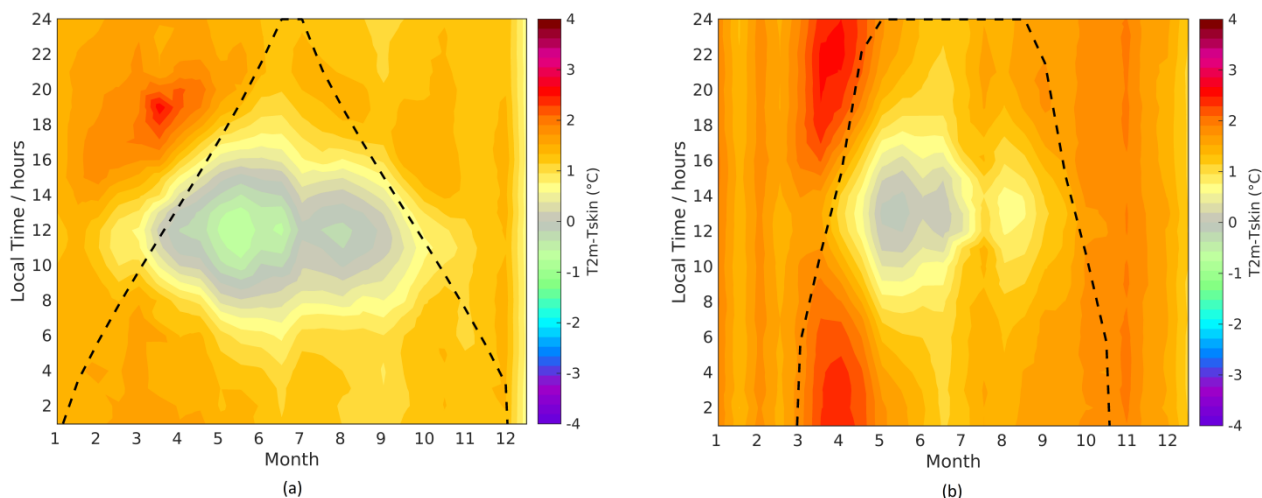


**Figure 7: Mean 2 m air temperature and skin temperature differences at KAN\_U (a) and KPC\_U (b) as a function of time of year (with a bin size of 15 days) and local time of the day. The dotted black lines indicate the total hours of sunlight.**

Figures 3-6 indicated both yearly and daily variations in the observed Tskin and T2m relationship. A detailed analysis of these variations can be seen in Figures 7a-b, which illustrate the mean diurnal and seasonal T2m-Tskin differences at two GrIS stations at different latitudes and altitudes (KAN\_U and KPC\_U). As also noticed in Fig. 3, the winter months have very little diurnal variability in the T2m-Tskin difference, with an approximately constant difference of about 1-2°C. During summer the difference decreases and the weakest vertical stratification is found close to the peak of the diurnal cycle, where Tskin may even exceed T2m slightly resulting in an unstable stratification of the surface air column. During night, the surface is often colder than the atmosphere and a surface-based inversion is established. The T2m-Tskin differences are generally higher at KPC\_U compared to KAN\_U, but they have similar variability throughout the year and day. This pattern is also recognized for the other stations.

#### 4.2 Impact from wind

The surface wind speed is an important component in the near surface thermal stratification due to the turbulent heat fluxes. In general, winds on the GrIS are strongest in winter and reach a minimum around July (Fig. 8; Steffen and Box, 2001). The surface radiative cooling and the terrain play the primary role in the generation of the surface winds (van As et al., 2014). The wind regimes differ among the observation sites used in this study. High elevation sites experience stronger winds due to the larger radiative cooling of the surface (provided a surface slope is present; Fig. 8; van As et al., 2014). The THU\_U site experiences wind speeds of about the same monthly mean magnitude all year around. Similar, the ARM and sea ice sites show less variability in wind speed on an annual basis. In general, the sea ice sites experience weaker winds.

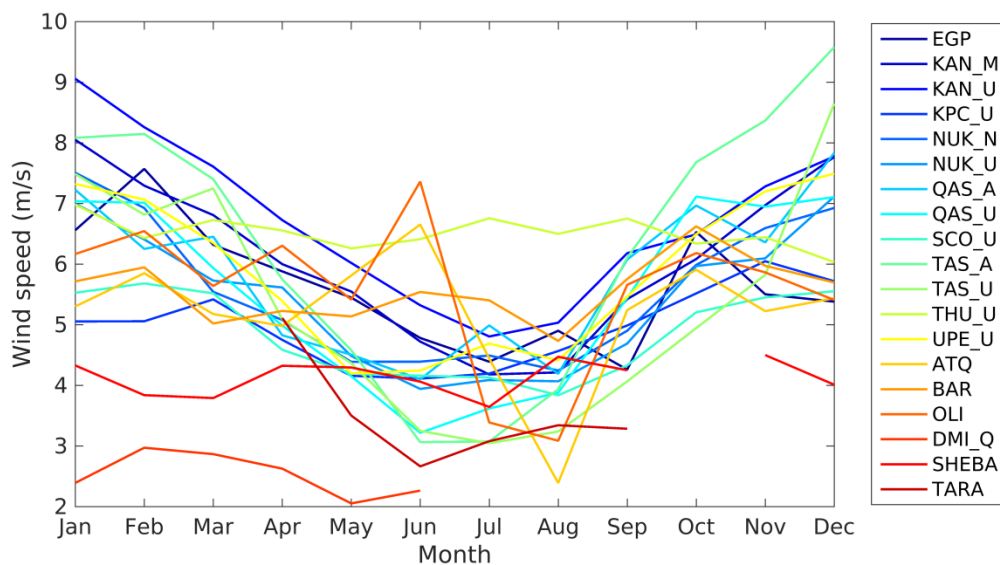


**Figure 8: The average annual cycle in wind speed for all sites.**

This section relates the surface-based temperature inversion to wind. The expectation is that stronger inversions can develop in low wind speed conditions because of reduced turbulent mixing. Figure 9a-b shows the T2m-Tskin difference as a function of binned wind speed with a bin size of  $0.5 \text{ m s}^{-1}$ . Only bins with more than 50 members are included. The number of members in each bin is shown in the bottom plots (blue curve) together with the cumulative percentage (red curve). The middle plots show the binned distribution of the T2m-Tskin difference (with bin size of 1 K) as a function of binned wind speed, where the colour bar is the number of matchups in each bin. The top plots show the mean (solid lines) and standard deviation (dashed lines) of the T2m-Tskin difference as a function of the binned wind speeds. Figure 9a shows data from the DMI\_Q AWS on sea ice. As expected, the strongest temperature inversion occurs at low wind speeds and larger wind speeds have larger turbulent mixing and thus smaller vertical temperature gradients between Tskin and T2m. However, THU\_U (Fig. 9b) shows that this relationship can sometimes be more complicated than that. At calm wind ( $<2.5 \text{ m s}^{-1}$ ) the mean and standard deviation reach a local minimum, and the inversion tend to be strongest around  $3\text{-}5 \text{ m s}^{-1}$ .

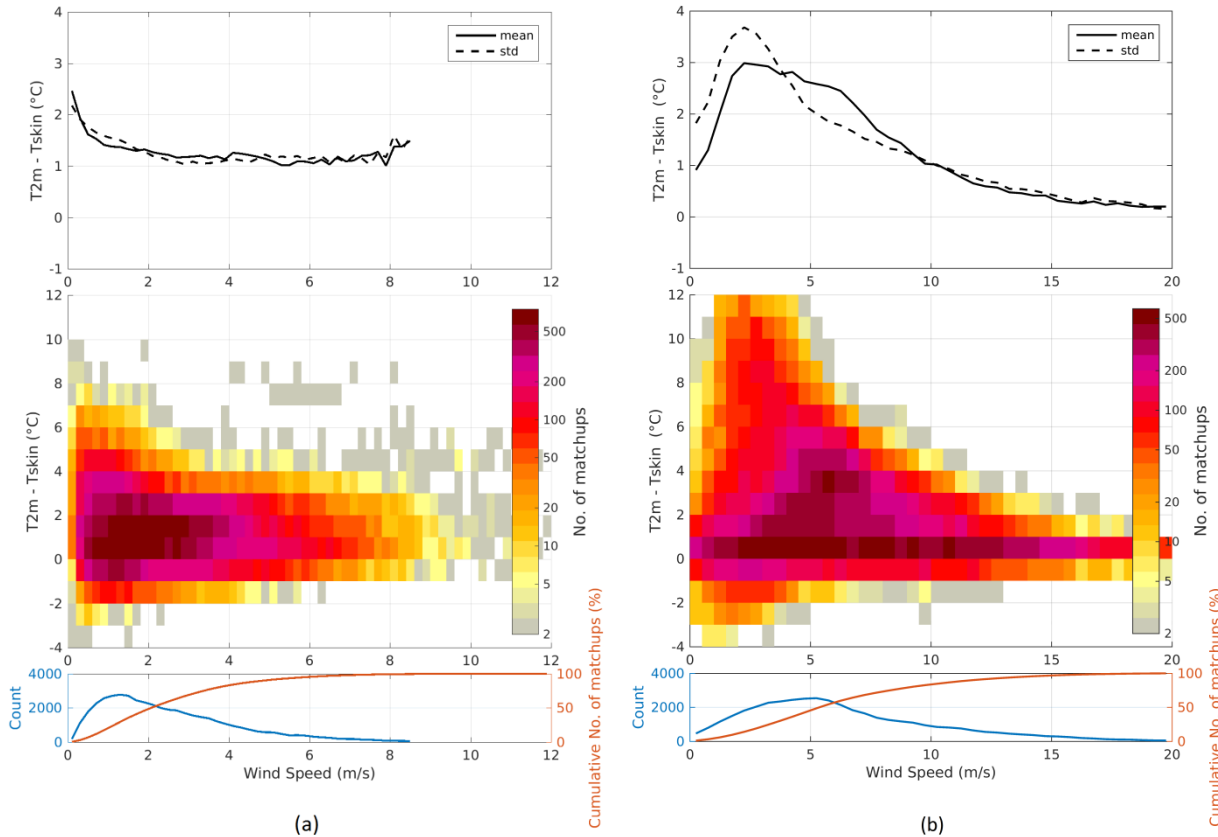


**Figure 9: 2 m air temperature and skin temperature difference as a function of binned wind speed for (a) DMI\_Q and (b) THU\_U. The upper plots show the standard deviation (dashed lines) and mean difference (solid lines). The middle plots show the number of matchups in each bin, while the bottom plots show the number of matchups (blue lines) and the cumulative percentage of matchups (red lines) in each wind speed bin.**

5

This behaviour is common for all PROMICE sites and is also found at the Summit station on the GrIS, where 2 m air temperature has been compared to IR skin temperature (Adolph et al., 2017). Miller et al. (2013) find that the surface based inversion intensity peaks at wind speeds ranging from 3 to 10 m s<sup>-1</sup> using microwave radiometer retrieved profiles at Summit. Also at the South Pole the maximum inversion tend to occur at wind of 3-5 m s<sup>-1</sup> and not calm winds considering the 22 m and 2 m air temperature difference (Hudson and Brandt, 2005). Hudson and Brandt suggest that it is not the weak wind of 3-5 m s<sup>-1</sup> that promotes strong inversion, but the inversion, which causes an inversion wind. They investigated this using the model by Mahrt and Schwerdtfeger (1970), which relates the slope of the terrain and the strength of the inversion to the inversion wind. Their results supported the idea that the inversion wind can explain the “unexpected” location of the maximum in inversion strength. These independent studies suggest that this might also be a real feature of the GrIS. It is likely that the GrIS represents a different case for inversion winds than for the interior of Antarctica due to Greenland’s smaller dimensions. However, it seems that the nature of the surface winds and the directional constancy are highly comparable between Antarctica and Greenland (van den Broeke et al., 1994; King and Turner, 1997).

10

15

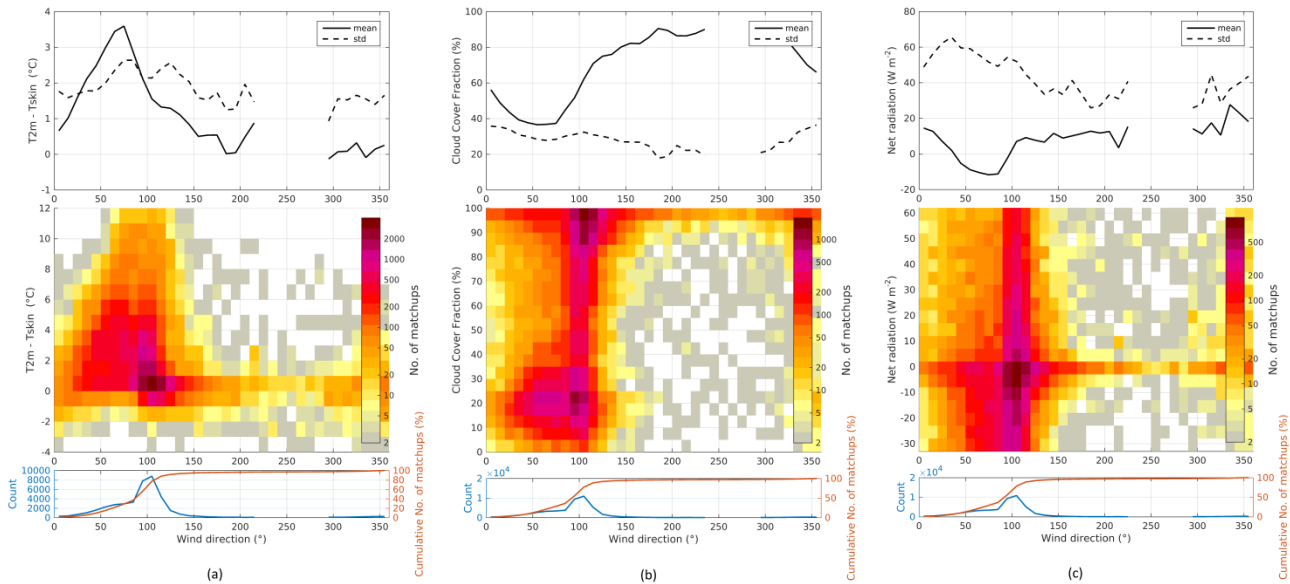


**Figure 10: 2 m air temperature and Tskin difference (a), the cloud cover fraction (b), and the net radiation (c) as a function of binned wind direction for THU\_U. The upper figures show the standard deviation (dashed lines) and mean difference (solid lines). The surface plots in the middle show the number of matchups in each bin, while the bottom plots show the number of matchups (blue lines) and the cumulative percentage of matchups (red lines) in each wind direction bin.**

5

Figure 10a shows the  $T_{2m} - T_{skin}$  difference plotted as a function of the wind direction at THU\_U. Nearly all measurements correspond to winds blowing from the upslope direction ( $55^\circ$  north-east) but deflected to the right ( $100^\circ$  south-east) due to the Coriolis force. The strongest inversion occurs at wind directions from  $25$ - $125^\circ$ . We find that the surface winds at the PROMICE sites in general have a high directional persistence (see also Fig. 4 in van As et al., 2014), commonly blowing from inland, which is a strong indication that local winds are often katabatic winds. This hypothesis is supported by Fig. 10b, which shows the wind direction as a function of the cloud cover fraction. Winds from the upslope direction are coincident with a minimum in the cloud cover fraction. The result is a negative surface net radiation (Fig. 10c), which allows a larger radiative cooling of Tskin and therefore a stronger inversion generating/driving the katabatic winds. These results support the idea by Hudson and Brandt (2005) that the inversion wind explains the maximum in inversion strength at about  $5 m s^{-1}$ .

10

15

It is outside the scope of this paper to fully explain all the features observed at the GrIS, but it is interesting to note that the unique environmental conditions and regional topography makes the GrIS different than the sites located on sea ice and land ice, with limited topography such as DMI\_Q, SHEBA, FRAM and the ARM sites.

### 4.3 Impact from clouds

The difference in  $LW_d$  radiation between clear-sky and overcast conditions can result in large differences in both  $T_{2m}$  and  $T_{skin}$  due to the effects on the surface radiation budget. In this section, we assess the inversion strength as a function of the cloud cover and in Sect. 4.3.1 a clear-sky bias is estimated for all sites.

20



Clear-sky conditions are defined to be cases with  $CCF < 30\%$ , while overcast conditions are defined to have  $CCF > 70\%$ . The frequency of clear-sky (overcast) observations is defined as the number of clear-sky (overcast) observations compared to the total number of observations. Figure 11 shows the frequency of clear-sky and overcast observations for each of the observation sites used in this study. The frequency of clear-sky observations ranges from 4 % at ATQ to 52 % at SCO\_U, while the frequency of overcast observations ranges from 25 % at SCO\_U to 63 % at DMI\_Q. Except for KAN\_M, SCO\_U and UPE\_U the frequency of overcast conditions is larger than the frequency of clear-sky observations at all sites.

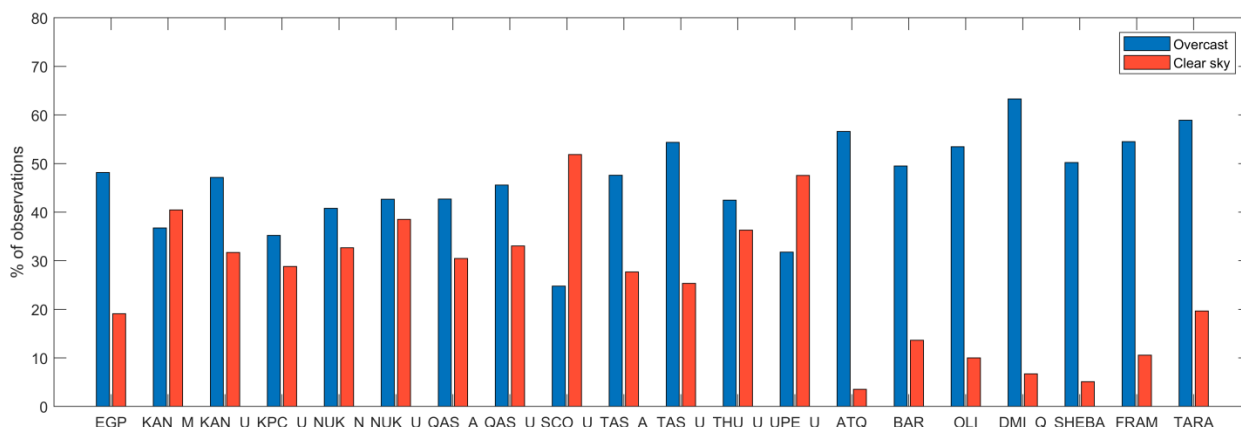


**Figure 11: Frequency of clear-sky and overcast observations in percent of all observations for each site.**

Similar to most PROMICE sites KAN\_U (Fig. 12a) shows the greatest frequency of clear-sky observations during the summer months and greatest frequency of overcast conditions during the winter months. The ARM site BAR (Fig. 12b) shows a year-round predominance of overcast conditions compared to clear-sky conditions.

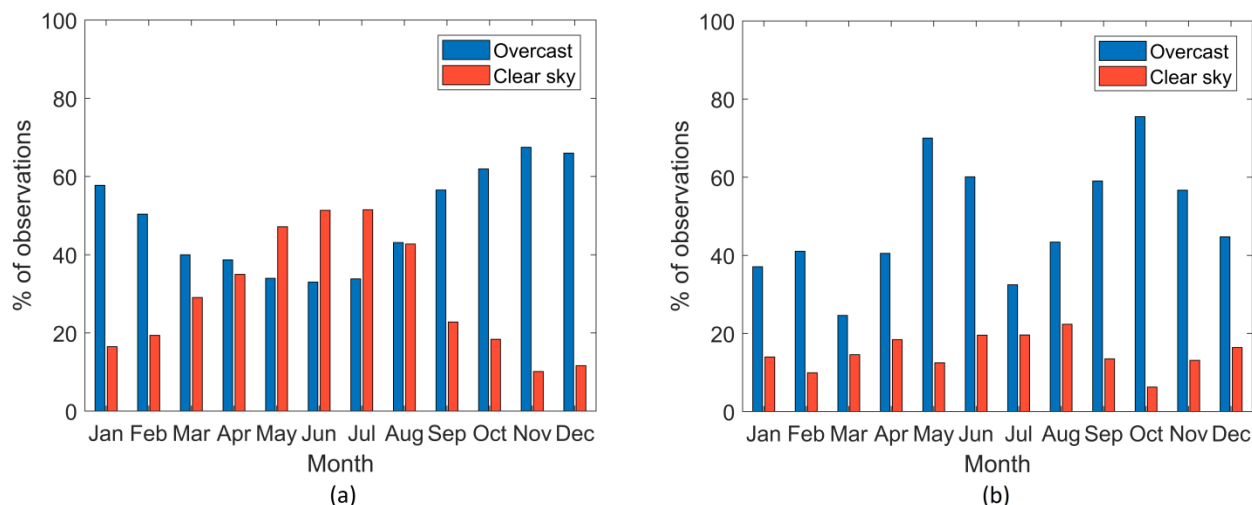


**Figure 12: Frequency of clear-sky and overcast conditions for each month at KAN\_U (a) and BAR (b).**



The relation between the inversion strength and CCF is shown in Fig 13, considering all sites. The bin size is 5 % and only bins with more than 50 members are considered. As expected, the obvious feature is that the inversion strength decreases with increasing  $LW_d$  radiation from a more extensive cloud cover. The observation sites show the strongest inversion during clear-sky conditions, reaching a mean value of 2.31°C for CCFs in the range 0-30%, considering all sites. Overcast conditions lead to a weaker inversion of 0.53°C considering all observations with a CCF of 70-100%. The average slope is -0.023K/% considering all sites.

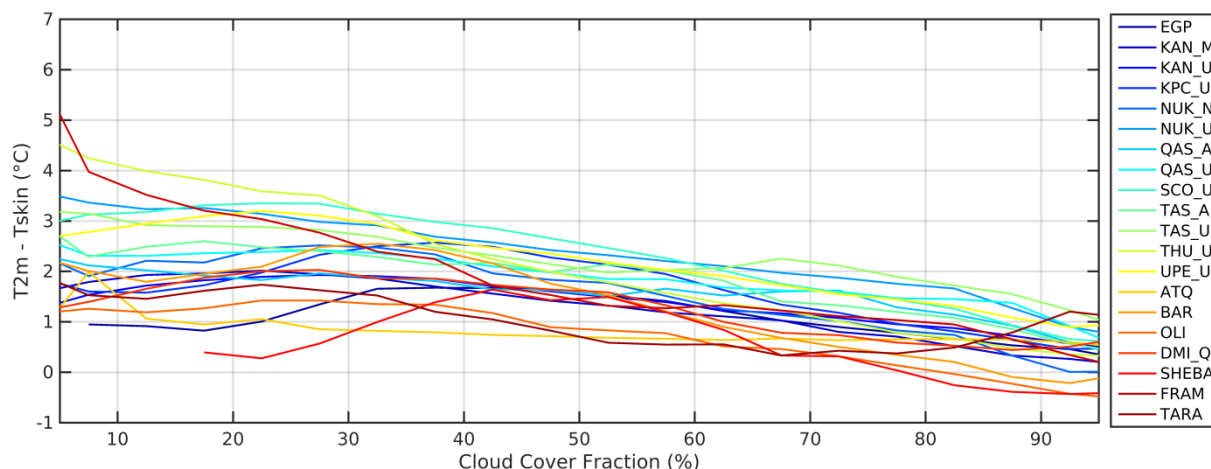


**Figure 13: 2 m air temperature and skin temperature differences for all sites as a function of cloud cover fraction.**

Figure 14a-b show how the temperature differences at KAN\_U vary as a function of season and local time for clear-sky and overcast conditions, respectively. Clear-sky conditions show the largest stratification with temperature differences up to 3°C during winter and night time. Overcast conditions reduce the temperature gradient at all times, with the largest temperature differences of about 1.5°C. During summer around noon, overcast conditions usually lead to an unstable stratification of the order of -1°C. An unstable stratification may also occur during clear-sky conditions and large solar insolation. This behaviour is common for all stations included in this study.

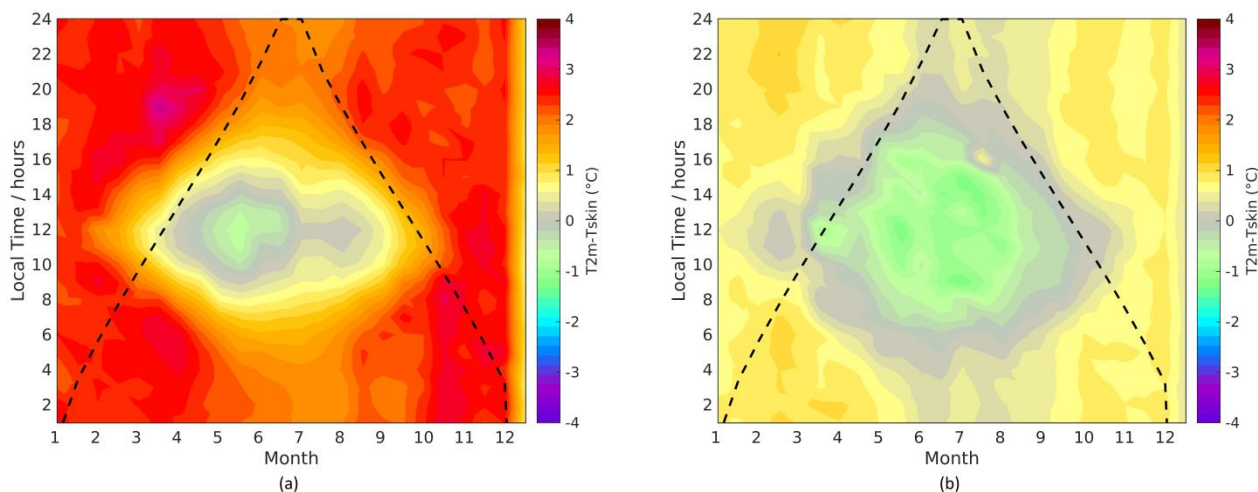


**Figure 14:** Similar to Fig. 7a but with 2 m air temperature and skin temperature differences at KAN\_U in cases of clear-sky (a), and overcast conditions (b). The dotted black lines indicate the total hours of sunlight each month.

**Table 2 Overall 2 m air temperature and skin temperature differences (T2m-Tskin, °C) for all sites (ALL), SEAICE+ (including the sea ice sites and ARM), and PROMICE under different circumstances in terms of season and sky conditions.**

	Jun-Aug			Dec-Feb			All		
	ALL	SEAICE+	PROMICE	ALL	SEAICE+	PROMICE	ALL	SEAICE+	PROMICE
Cloud	0.58	0.30	0.73	0.57	0.09	0.79	0.53	0.31	0.65
Clear	1.94	1.86	1.97	2.90	2.09	3.24	2.31	1.98	2.46
All	1.29	0.73	1.58	1.50	0.89	1.78	1.37	0.88	1.64

Figure 14 demonstrates the factors that influence the T2m-Tskin differences, such as day of year, time of day and cloud cover. The impact of this variability for all stations is quantified in Table 2, which summarizes the findings of the dependencies of cloud/clear and summer/winter on the T2m-Tskin difference for all sites (ALL), a division into SEAICE+, which includes the Arctic sea ice sites and the ARM sites, and PROMICE sites, all sites weighted equal. In general, the SEAICE+ sites show a weaker inversion than the PROMICE sites. In all cases and for all times of the year, cloud cover tends to decrease the inversion strength. Both groups of stations experience the strongest inversion during winter clear-sky conditions.

### 15 4.3.1 Clear-sky bias

The most accurate surface temperature satellite observations are thermal IR observations that can only be observed during clear-sky conditions. This fact will potentially introduce a clear-sky bias when satellites are used to estimate the average



Tskin. To facilitate the use of satellite observations it is therefore important to get a measure of the influence of clouds on Tskin. As the satellite IR observations have gaps in cloudy conditions, the satellite Tskin products are often averages over a given time window (see e.g. Rasmussen et al., 2018). When using the averaged Tskin observations for monitoring or in combination with ocean-sea ice or atmospheric models, it is therefore important to assess the impact of temporal averaging window on the clear-sky bias. The clear-sky bias has been assessed by comparing clear-sky Tskin observations with all-sky Tskin observations, averaged for different time windows: 24 h, 72 h and 1 month, for all sites. The results are shown in Fig. 15. The average clear-sky biases are  $-0.28^{\circ}\text{C}$ ,  $-0.36^{\circ}\text{C}$  and  $-1.40^{\circ}\text{C}$  using the time windows 24 h, 72 h and 1 month, respectively. For most stations all-sky observations are warmer than clear-sky observations for all time windows. However, there is large variability among the stations and at a few stations e.g. EGP, ATQ and DMI\_Q the all-sky observations are colder than clear-sky observations using the 24 h and/or 1 month time windows. The top panels of Fig. 16 show the mean difference in 24 h averaged clear-sky and all-sky Tskin for the PROMICE stations (a) and the SEAICE+ sites (b), averaged for each month. For both groups of stations it is found that the 24 h averaged clear-sky bias is smaller during summer (ALL:  $-0.10^{\circ}\text{C}$ ; SEAICE+:  $-0.19^{\circ}\text{C}$ ; PROMICE:  $-0.05^{\circ}\text{C}$ ) than winter (ALL:  $-0.95^{\circ}\text{C}$ ; SEAICE+:  $-0.42^{\circ}\text{C}$ ; PROMICE:  $-1.26^{\circ}\text{C}$ ), which may be a result of the smaller daily Tskin range in summer (Fig. 5). The SEAICE+ stations have an overall positive clear-sky bias of  $0.79^{\circ}\text{C}$  in spring. The bottom panels of Fig. 16 show the amount of hours with clouds (CCF>70%) per day, averaged for each month. Both groups of stations have a minimum in the hours with cloud cover during summer. On average the SEAICE+ sites have about 4 h more with clouds per day compared to the PROMICE stations. EGP has no clear-sky observations in Dec.-Feb. and at DMI\_Q clear-sky observations are only available Feb.-Jun., which may explain the overall positive 24 h clear-sky bias observed in Fig. 15. The 72 h and 1 month averaged clear-sky biases show the same seasonal variation as in Fig. 16, with the smallest biases in summer and largest biases in winter.

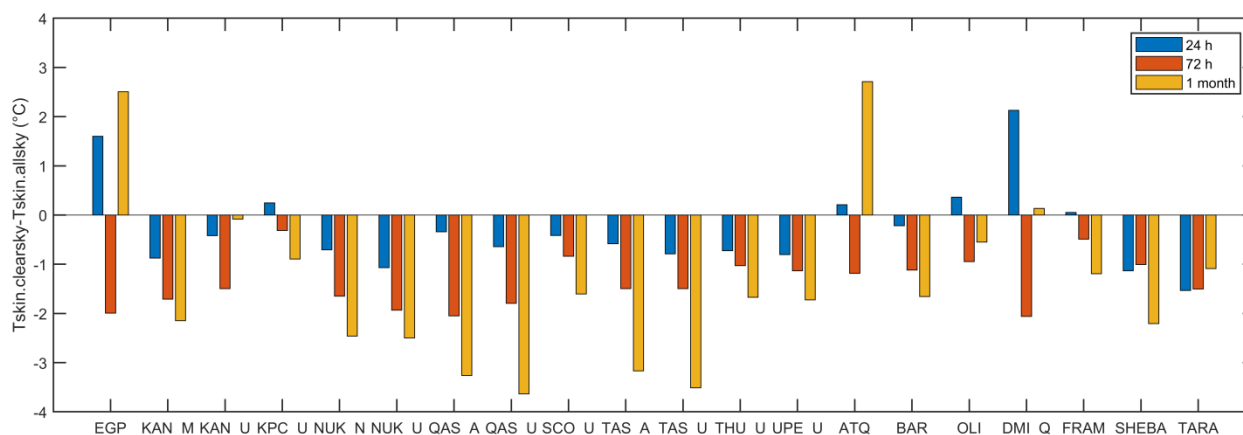


**Figure 15: Observed clear-sky biases ( $T_{skin\_clearsky} - T_{skin\_allsky}$ ) averaged for different time intervals, for all sites ( $^{\circ}\text{C}$ ).**

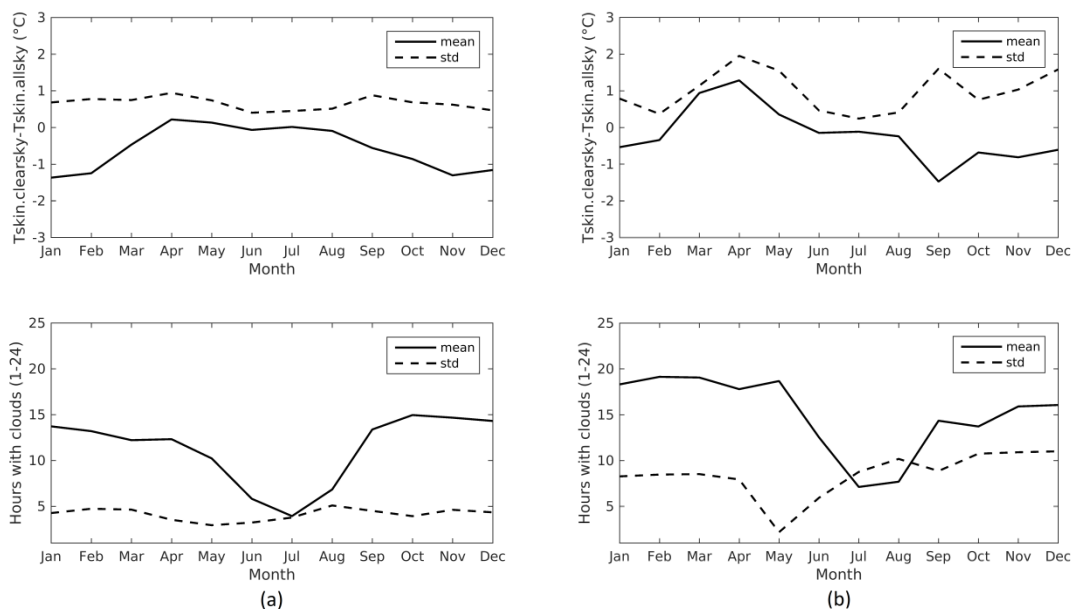


**Figure 16:** The top panels show the differences between 24 h averaged clear-sky and all-sky skin temperatures for PROMICE stations (a) and SEAICE+ stations (b) for each month. The solid lines are the mean clear-sky bias while the dashed lines are standard deviations. The bottom panels show the 24 h averaged number of hours with CCF > 70% per day for each month.

#### 5 4.4 Relationship with skin surface temperature

Section 4.3 showed how clouds impact the T<sub>2m</sub> and T<sub>skin</sub> relationship, and Sect. 4.3.1 revealed a close relationship between T<sub>skin</sub> and the CCF. In reality it is, however, difficult to obtain reliable observations of cloud cover from the entire Arctic using, e.g. satellite observations. This section therefore investigates how the T<sub>2m</sub>-T<sub>skin</sub> difference is related to the skin temperature itself. The relationship with T<sub>skin</sub> is corroborated in Fig. 17 where the strength of the surface-based inversion is shown as a function of T<sub>skin</sub>. The T<sub>skin</sub> bin size is 1°C and only bins with more than 50 members are considered. All PROMICE sites show an almost linear trend towards weaker inversion strength for warmer skin temperatures with the steepest slope of the curve for low elevation sites. Strong trends are also seen for BAR, SHEBA, TARA and DMI\_Q. ATQ and OLI show a similar but weaker trend, while FRAM shows an opposite trend with larger T<sub>2m</sub>-T<sub>skin</sub> differences for higher skin temperatures. However, the standard deviation (not shown) decreases for higher temperatures for FRAM. The average slope of the curve for all stations except FRAM is -0.055 K/K. The results of this section can be useful to relate T<sub>skin</sub> to T<sub>2m</sub> in situations, where the cloud cover and longwave radiation are not available.

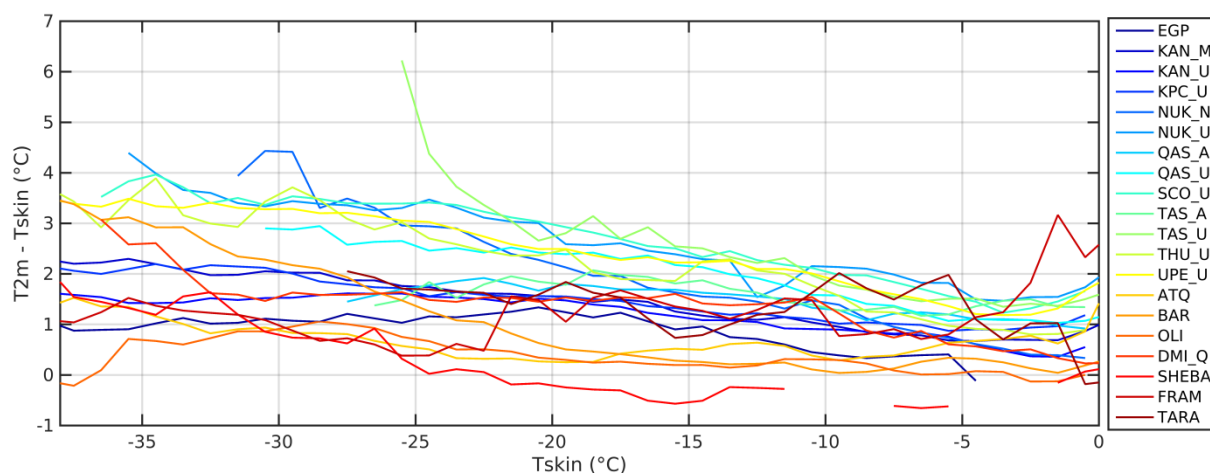


**Figure 17: Mean 2 m air temperature and skin temperature differences for all sites as a function of skin temperature.**

## 5 Discussion

The initial study on the T2m and Tskin variability shows that the coldest month ranges from December to March, whereas the warmest month is July for all sites considering both Tskin and T2m. This is in agreement with mean air temperatures found in Steffen and Box (2001) for Greenland GC-Net AWSs, Persson (2002) for Arctic sea ice and Rigor et al. (2000) for North Pole stations and land stations in Alaska. The monthly mean daily temperature range is largest in April-May and reaches a minimum in July, related to the upper temperature limit when the ice or snow is melting. Surface temperature inversions are very common for the Arctic region. Considering the sites included in this analysis, the mean temperature difference between T2m and Tskin is 1.37°C with the strongest inversion over the GrIS (1.64°C) compared to the sites in Alaska and on the Arctic sea ice (0.88°C). Inversions are predominantly found during winter (low-sun and polar night periods), which allows for a strong radiative cooling at the surface. Smaller temperature differences are dominating in spring and summer, around noon and early afternoon, where the sun is warming the surface. This is in agreement with Adolph et al. (2017) that found large T2m-Tskin differences during night time and small differences during the peak solar irradiance (see Fig. 5 in Adolph et al., 2017). During summer and local noon Tskin exhibits the closest coupling to T2m and the satellite observed Tskin observations will therefore have the best agreement with the T2m at these times.

Increasing wind speeds are expected to decrease the inversion strength through increased turbulence, mixing warmer air downwards. This is also seen at the ARM sites and Arctic sea ice sites, where the strongest inversion occurs at calm winds and weaker inversions occur with increasing wind speed. Although the effect from wind speed seems easy to understand, the relationship has turned out to be more complicated than that at sites with a sloping terrain. All sites on the GrIS showed a unique feature with the maximum inversion strength at winds of about 5 m s<sup>-1</sup> and not at calm winds. This feature has previously been identified by a few others in Antarctica (Hudson and Brandt, 2005) and at Summit, GrIS (Miller et al.,



2013). The feature is also noticed at Summit in Figure 7 in Adolph et al., (2017). It is likely that this feature is driven by the inversion/katabatic winds. The inversion/katabatic winds blow persistently perpendicular to the fall line of the terrain, with a speed related to the magnitude of the slope but also other factors such as the strength of the inversion, the velocity of the wind above the inversion layer, surface friction, Coriolis force, and gravity. Hudson and Brandt (2005) performed an analysis on the surface wind resulting from the inversion over sloped terrain and found that the inversion can induce winds of this magnitude at the South Pole, suggesting that this may be why the maximum inversions occur at non-zero wind speeds. We find that all PROMICE sites show persistent winds blowing from the upslope direction and deflected to the right (see also Fig. 4 in van As et al., 2014). We also find that the downslope winds typically occur during cloud-free conditions, which result in a strong radiative cooling of the surface and therefore a more negative net radiation at the surface. It is likely that the GrIS represents a different case for inversion winds than for the interior of Antarctica due to Greenland's smaller dimensions, but it does seem like the nature of the surface winds and the directional persistence found in Antarctica are comparable to the results found here for the GrIS. More research is needed to completely understand and explain the impact of wind on the inversion, and vice versa.

The analysis of the impact of clouds showed an almost linear relationship between cloud cover and the T2m-Tskin difference, with a trend towards zero with increasing CCF (Fig. 13). Also the variability of the inversion strength tends to decrease with increasing CCF (not shown). Considering all sites the T2m-Tskin difference decreases from an all-sky value of 1.37°C to 0.53°C considering observations with a CCF above 70 %. On the other hand, the difference increases to 2.31°C by only considering observations with CCFs below 30 %. The explanation is that clouds in the Arctic have a predominantly warming effect on the surface (Intrieri, 2002; Walsh and Chapman, 1998). In cases where the cloud cover and longwave radiation are not available, the T2m and Tskin relationship can be quantified by using the Tskin instead. We have found an almost linear relationship between the inversion strength and the skin temperatures, with weaker inversions for higher Tskin. This is in agreement with Adolph et al. (2017) that finds larger T2m-Tskin differences at lower temperatures at the Summit station, during summer.

To assess if there are any impact of clear-sky observations on the radiometer observations due to the different spectral characteristics (broad band versus narrow band, as discussed in Sect. 2.7), the T2m-Tskin differences as a function of CCF were calculated for narrow band Tskin and broad band Tskin for the stations containing both instruments (ATQ, BAR, OLI, DMI\_Q, SHEBA, and FRAM). This resulted in a very small change in the slope from -0.025 to -0.022 for narrow band and broad band Tskin estimates, respectively. Similarly, the T2m-Tskin differences were calculated for both types of radiometers as a function of Tskin. Again, the change in trend was small from -0.045 to -0.052, excluding the FRAM site as in Sect. 4.4. The influence of clouds on Tskin has been assessed by comparing clear-sky Tskin observations with all-sky Tskin observations averaged for different time intervals: 24 h, 72 h and 1 month, for all sites. In general, the cloud-free only monthly average is colder than the true monthly average with a mean clear-sky bias of -0.28°C using the 24 h time interval. The clear-sky bias tends to increase with the length of the time interval used for averaging, but the clear-sky biases vary among the stations. However, the frequency of clear-sky observations also varies a lot among the stations with SEAICE+



stations having a clear-sky frequency of 10 % compared to the PROMICE stations with a clear-sky frequency of 34 % (Fig. 11). In general, the clear-sky bias is smaller during summer than winter for all averaging windows. This is also reported by Comiso (2000), who finds a monthly mean clear-sky bias of about  $-0.3^{\circ}\text{C}$  during summer (Jan.) and  $-0.5^{\circ}\text{C}$  during winter (Jul.) at Antarctic stations. The range in temperature over the averaging window as well as the frequency and timing of clear-sky observations are thought to play an important role in the clear-sky bias variations observed among the stations.

5 The observed clear-sky bias explains part of the cold-bias observed in IR satellite retrievals of skin surface temperature compared to in situ surface temperatures (Høyer et al., 2017; Rasmussen et al., 2018; Shuman et al., 2014). Another part of the explanation is related to the fact that the in situ “surface” air temperature measured at the surface, typically is measured at about 2 m height. The significant temperature gradients in the lowest 2 m of the atmosphere mean that satellite retrievals

10 of surface temperature will be colder than the in situ measurements at 2 m height.

## 6 Conclusions

Coincident in situ skin temperature ( $T_{\text{skin}}$ ) and 2 m air temperatures ( $T_{2\text{m}}$ ) from 20 deployments in the Arctic region have been analysed to assess the variability and the factors controlling the  $T_{\text{skin}}$  and  $T_{2\text{m}}$  variations in order to facilitate the combined use of satellite observed  $T_{\text{skin}}$  and traditional observations of  $T_{2\text{m}}$ . The main factors that influence the  $T_{\text{skin}}$  and

15  $T_{2\text{m}}$  relationship include seasonal variations, wind speed, and cloud cover. The extensive data sets gathered in this study represent a wide range of weather conditions, from melting sea ice in the summer, over land based Arctic stations to high altitude sites on the GrIS. Historical and present in situ records consist to a large degree of a limited set of  $T_{2\text{m}}$  observations. Conversely, satellite observations can provide global coverage on a daily basis of clear-sky  $T_{\text{skin}}$ . There is thus a large potential in combining these types of observations either for satellite validation purposes or for extension of the time series

20 in space and time, but this requires a detailed knowledge and quantification of the relationship between  $T_{\text{skin}}$  and  $T_{2\text{m}}$  and of the factors determining the relationships. It is our hope that this study has contributed to a better understanding of the relationships.

## 7 Author contribution

Pia Nielsen-Englyst and Kristine S. Madsen compiled and quality checked the in situ data. Pia Nielsen-Englyst, Jacob L.

25 Høyer and Kristine S. Madsen designed the experiments and Pia Nielsen-Englyst carried them out. Pia Nielsen-Englyst prepared the manuscript with contributions from all authors.

## 8 Competing interests

The authors declare that they have no conflict of interest.



## 9 Acknowledgements

This study was carried out as a part of the European Union Surface Temperatures for All Corners of Earth (EUSTACE), which is financed by the European Union's Horizon 2020 Programme for Research and Innovation, under Grant Agreement no 640171. The aim of EUSTACE is to provide a spatially complete daily field of air temperatures since 1850 by combining  
5 satellite and in situ observations. The author would like to thank the data providers. Data was provided by PROMICE, which is funded by the Danish Ministry of Climate, Energy and Building, operated by the Geological Survey of Denmark and Greenland and conducted in collaboration with the National Space Institute (DTU Space) and Asiaq (Greenland Survey). Data were also obtained from the Atmospheric Radiation Measurement (ARM) Climate Research Facility, a U.S.  
10 Department of Energy Office of Science user facility sponsored by the Office of Biological and Environmental Research. We thank our colleagues in the SHEBA Atmospheric Surface Flux Group, Ed Andreas, Chris Fairall, Peter Guest, and Ola Persson for help collecting and processing the data. The National Science Foundation supported this research with grants to the U.S. Army Cold Regions Research and Engineering Laboratory, NOAA's Environmental Technology Laboratory, and the Naval Postgraduate School. Data was also provided by Timo Palo from the Tara expedition, supported by the European Commission 6th Framework Integrated Project DAMOCLES and in part by the Academy of Finland through the CACSI  
15 project. Finally, we thank Steinar Eastwood from the Norwegian Meteorological Institute for providing us with data from the FRAM2014/15 expedition.

## References

- Abermann, J., Hansen, B., Lund, M., Wacker, S., Karami, M. and Cappelen, J.: Hotspots and key periods of Greenland climate change during the past six decades, *Ambio*, 46(S1), 3–11, doi:10.1007/s13280-016-0861-y, 2017.
- 20 Ackerman, T. P. and Stokes, G. M.: The Atmospheric Radiation Measurement Program, *Phys. Today*, 56(1), 38–44, doi:10.1063/1.1554135, 2003.
- Adolph, A. C., Albert, M. R. and Hall, D. K.: Near-surface thermal stratification during summer at Summit, Greenland, and its relation to MODIS-derived surface temperatures, *Cryosphere Discuss.*, 1–24, doi:10.5194/tc-2017-195, 2017.
- Ahlstrøm, A., van As, D., Citterio, M., Andersen, S., Fausto, R., Andersen, M., Forsberg, R., Stenseng, L., Lintz  
25 Christensen, E. and Kristensen, S. S.: A new Programme for Monitoring the Mass Loss of the Greenland Ice Sheet, *Geol. Surv. Den. Greenl. Bull.*, 15, 61–64, 2008.
- van As, D.: Warming, glacier melt and surface energy budget from weather station observations in the Melville Bay region of northwest Greenland, *J. Glaciol.*, 57(202), 208–220, doi:10.3189/002214311796405898, 2011.
- van As, D., Broeke, M. van den, Reijmer, C. and Wal, R. van de: The Summer Surface Energy Balance of the High Antarctic  
30 Plateau, *Bound.-Layer Meteorol.*, 115(2), 289–317, doi:10.1007/s10546-004-4631-1, 2005.
- van As, D., Fausto, R., Steffen, K., Ahlstrøm, A., Andersen, S. B., Andersen, M. L., Box, J., Charalampidis, C., Citterio, M., Colgan, W. T., Edolvang, K., Larsen, S. H., Nielsen, S., Martin, V. and Weidick, A.: Katabatic winds and piteraq storms: Observations from the Greenland ice sheet, *Geol. Surv. Den. Greenl. Bull.*, (31), 83–86, 2014.
- Box, J. E., Fettweis, X., Stroeve, J. C., Tedesco, M., Hall, D. K. and Steffen, K.: Greenland ice sheet albedo feedback: thermodynamics and atmospheric drivers, *The Cryosphere*, 6(4), 821–839, doi:10.5194/tc-6-821-2012, 2012.
- Bretherton, C. S., Roode, S. R. de, Jakob, C., Andreas, E. L., Intrieri, J., Moritz, R. E. and Persson, O. G.: A comparison of the ECMWF forecast model with observations over the annual cycle at SHEBA. Unpublished manuscript, 2000.



- van den Broeke, M., Duynkerke, P. and Oerlemans, J.: The observed katabatic flow at the edge of the Greenland ice sheet during GIMEX-91, *Glob. Planet. Change*, 9(1–2), 3–15, doi:10.1016/0921-8181(94)90003-5, 1994.
- Cappelen, J.: Greenland—DMI Historical Climate Data Collection 1784–2015. Danish Meteorological Institute., 2016.
- Cohen, J., Screen, J. A., Furtado, J. C., Barlow, M., Whittleston, D., Coumou, D., Francis, J., Dethloff, K., Entekhabi, D., Overland, J. and Jones, J.: Recent Arctic amplification and extreme mid-latitude weather, *Nat. Geosci.*, 7(9), 627–637, doi:10.1038/ngeo2234, 2014.
- Comiso, J. C.: Variability and Trends in Antarctic Surface Temperatures from In Situ and Satellite Infrared Measurements, *J. Clim.*, 13(10), 1674–1696, doi:10.1175/1520-0442(2000)013<1674:VATIAS>2.0.CO;2, 2000.
- Curry, J. A. and Herman, G. F.: Infrared Radiative Properties of Summertime Arctic Stratus Clouds, *J. Clim. Appl. Meteorol.*, 24(6), 525–538, doi:10.1175/1520-0450(1985)024<0525:IRPOSA>2.0.CO;2, 1985.
- Curry, J. A., Schramm, J. L., Rossow, W. B. and Randall, D.: Overview of Arctic Cloud and Radiation Characteristics, *J. Clim.*, 9(8), 1731–1764, doi:10.1175/1520-0442(1996)009<1731:OOACAR>2.0.CO;2, 1996.
- Dozier, J. and Warren, S. G.: Effect of viewing angle on the infrared brightness temperature of snow, *Water Resour. Res.*, 18(5), 1424–1434, doi:10.1029/WR018i005p01424, 1982.
- 15 Dybkjær, G., Tonboe, R. and Høyer, J. L.: Arctic surface temperatures from Metop AVHRR compared to in situ ocean and land data, *Ocean Sci.*, 8(6), 959–970, doi:10.5194/os-8-959-2012, 2012.
- Franco, B., Fettweis, X. and Erpicum, M.: Future projections of the Greenland ice sheet energy balance driving the surface melt, *The Cryosphere*, 7(1), 1–18, doi:10.5194/tc-7-1-2013, 2013.
- 20 Gascard, J.-C., Festy, J., le Goff, H., Weber, M., Bruemmer, B., Offermann, M., Doble, M., Wadhams, P., Forsberg, R., Hanson, S., Skourup, H., Gerland, S., Nicolaus, M., Metaxian, J.-P., Grangeon, J., Haapala, J., Rinne, E., Haas, C., Wegener, A., Heygster, G., Jakobson, E., Palo, T., Wilkinson, J., Kaleschke, L., Claffey, K., Elder, B. and Bottenheim, J.: Exploring Arctic Transpolar Drift During Dramatic Sea Ice Retreat, *Eos Trans. Am. Geophys. Union*, 89(3), 21, doi:10.1029/2008EO030001, 2008.
- Good, E. J., Ghent, D. J., Bulgin, C. E. and Remedios, J. J.: A spatiotemporal analysis of the relationship between near-surface air temperature and satellite land surface temperatures using 17 years of data from the ATSR series, *J. Geophys. Res. Atmospheres*, 122(17), 9185–9210, doi:10.1002/2017JD026880, 2017.
- 25 Graversen, R. G., Mauritsen, T., Tjernström, M., Källén, E. and Svensson, G.: Vertical structure of recent Arctic warming, *Nature*, 451(7174), 53–56, doi:10.1038/nature06502, 2008.
- Hall, D., Box, J., Casey, K., Hook, S., Shuman, C. and Steffen, K.: Comparison of satellite-derived and in-situ observations of ice and snow surface temperatures over Greenland, *Remote Sens. Environ.*, 112(10), 3739–3749, doi:10.1016/j.rse.2008.05.007, 2008.
- 30 Hansen, J., Ruedy, R., Sato, M. and Lo, K.: Global surface temperature change, *Rev. Geophys.*, 48(4), doi:10.1029/2010RG000345, 2010.
- Høyer, J. L., Lang, A. M., Tonboe, R., Eastwood, S., Wimmer, W. and Dybkjær, G.: Towards field inter-comparison experiment (FICE) for ice surface temperature (ESA Tech. Rep. FRM4STS OP-40)., [online] Available from: <http://www.frm4sts.org/wp-content/uploads/sites/3/2017/12/OFE-OP-40-TR-5-V1-Iss-1-Ver-1-Signed.pdf>, 2017.



- Hudson, S. R. and Brandt, R. E.: A Look at the Surface-Based Temperature Inversion on the Antarctic Plateau, *J. Clim.*, 18(11), 1673–1696, doi:10.1175/JCLI3360.1, 2005.
- Intrieri, J. M.: An annual cycle of Arctic surface cloud forcing at SHEBA, *J. Geophys. Res.*, 107(C10), doi:10.1029/2000JC000439, 2002.
- 5 Jones, P. D., Lister, D. H., Osborn, T. J., Harpham, C., Salmon, M. and Morice, C. P.: Hemispheric and large-scale land-surface air temperature variations: An extensive revision and an update to 2010., *J. Geophys. Res. Atmospheres*, 117(D5), n/a-n/a, doi:10.1029/2011JD017139, 2012.
- King, J. C. and Turner, J.: *Antarctic Meteorology and Climatology*, Cambridge University Press, Cambridge., 1997.
- Koenig, L. S. and Hall, D. K.: Comparison of satellite, thermochron and air temperatures at Summit, Greenland, during the winter of 2008/09, *J. Glaciol.*, 56(198), 735–741, doi:10.3189/002214310793146269, 2010.
- 10 Kristoffersen, Y. and Hall, J.: Hovercraft as a Mobile Science Platform Over Sea Ice in the Arctic Ocean, *Oceanography*, 27(2), doi:10.5670/oceanog.2014.33, 2014.
- Lettau, H. H. and W. Schwerdtfeger: Dynamics of the surface-wind regime over the interior of Antarctica, *Antarct. J. U. S.*, 2(5), 155–158, 1967.
- 15 Mahrt, L. J. and Schwerdtfeger, W.: Ekman spirals for exponential thermal wind, *Bound.-Layer Meteorol.*, 1(2), 137–145, doi:10.1007/BF00185735, 1970.
- Masson-Delmotte, V., Swingedouw, D., Landais, A., Seidenkrantz, M.-S., Gauthier, E., Bichet, V., Massa, C., Perren, B., Jomelli, V., Adalgeirsdottir, G., Hesselbjerg Christensen, J., Arneborg, J., Bhatt, U., Walker, D. A., Elberling, B., Gillet-Chaulet, F., Ritz, C., Gallée, H., van den Broeke, M., Fettweis, X., de Vernal, A. and Vinther, B.: Greenland climate change: from the past to the future: Greenland climate change, *Wiley Interdiscip. Rev. Clim. Change*, 3(5), 427–449, doi:10.1002/wcc.186, 2012.
- 20 Maykut, G. A.: The Surface Heat and Mass Balance, in *The Geophysics of Sea Ice*, edited by N. Untersteiner, pp. 395–463, Springer US, Boston, MA., 1986.
- Miller, N. B., Turner, D. D., Bennartz, R., Shupe, M. D., Kulie, M. S., Cadeddu, M. P. and Walden, V. P.: Surface-based inversions above central Greenland, *J. Geophys. Res. Atmospheres*, 118(2), 495–506, doi:10.1029/2012JD018867, 2013.
- 25 Moris, V. R.: *Infrared Thermometer (IRT) Handbook Atmospheric Radiation Measurement publication ARM TR-015* available from <https://www.arm.gov/instruments/irt>, 2006.
- Pérez Díaz, C. L., Lakhankar, T., Romanov, P., Muñoz, J., Khanbilvardi, R. and Yu, Y.: Near-surface air temperature and snow skin temperature comparison from CREST-SAFE station data with MODIS land surface temperature data, *Hydrol. Earth Syst. Sci. Discuss.*, 12(8), 7665–7687, doi:10.5194/hessd-12-7665-2015, 2015.
- 30 Persson, P. O. G.: Measurements near the Atmospheric Surface Flux Group tower at SHEBA: Near-surface conditions and surface energy budget, *J. Geophys. Res.*, 107(C10), doi:10.1029/2000JC000705, 2002.
- Rasmussen, T. A. S., Høyer, J. L., Ghent, D., Bulgin, C. E., Dybkjaer, G., Ribergaard, M. H., Nielsen-Englyst, P. and Madsen, K. S.: Impact of Assimilation of Sea-Ice Surface Temperatures on a Coupled Ocean and Sea-Ice Model, *J. Geophys. Res. Oceans*, 123(4), 2440–2460, doi:10.1002/2017JC013481, 2018.
- 35



- Rayner, N. A.: Global analyses of sea surface temperature, sea ice, and night marine air temperature since the late nineteenth century, *J. Geophys. Res.*, 108(D14), doi:10.1029/2002JD002670, 2003.
- Reeves Eyre, J. E. J. and Zeng, X.: Evaluation of Greenland near surface air temperature datasets, *The Cryosphere*, 11(4), 1591–1605, doi:10.5194/tc-11-1591-2017, 2017.
- 5 Rigor, I. G., Colony, R. L. and Martin, S.: Variations in Surface Air Temperature Observations in the Arctic, 1979–97, *J. Clim.*, 13(5), 896–914, doi:10.1175/1520-0442(2000)013<0896:VISATO>2.0.CO;2, 2000.
- Screen, J. A. and Simmonds, I.: The central role of diminishing sea ice in recent Arctic temperature amplification, *Nature*, 464(7293), 1334–1337, doi:10.1038/nature09051, 2010.
- Serreze, M. C. and Francis, J. A.: The Arctic Amplification Debate, *Clim. Change*, 76(3–4), 241–264, doi:10.1007/s10584-10  
005-9017-y, 2006.
- Serreze, M. C., Schnell, R. C. and Kahl, J. D.: Low-Level Temperature Inversions of the Eurasian Arctic and Comparisons with Soviet Drifting Station Data, *J. Clim.*, 5(6), 615–629, doi:10.1175/1520-0442(1992)005<0615:LLTIOT>2.0.CO;2, 1992.
- Shuman, C. A., Hall, D. K., DiGirolamo, N. E., Mefford, T. K. and Schnaubelt, M. J.: Comparison of Near-Surface Air  
15 Temperatures and MODIS Ice-Surface Temperatures at Summit, Greenland (2008–13), *J. Appl. Meteorol. Climatol.*, 53(9), 2171–2180, doi:10.1175/JAMC-D-14-0023.1, 2014.
- Stamnes, K., Ellingson, R. G., Curry, J. A., Walsh, J. E. and Zak, B. D.: Review of Science Issues, Deployment Strategy, and Status for the ARM North Slope of Alaska–Adjacent Arctic Ocean Climate Research Site, *J. Clim.*, 12(1), 46–63, doi:10.1175/1520-0442-12.1.46, 1999.
- 20 Steffen, K. and Box, J.: Surface climatology of the Greenland Ice Sheet: Greenland Climate Network 1995–1999, *J. Geophys. Res. Atmospheres*, 106(D24), 33951–33964, doi:10.1029/2001JD900161, 2001.
- Swinbank, W. C.: Long-wave radiation from clear skies, *Q. J. R. Meteorol. Soc.*, 89(381), 339–348, doi:10.1002/qj.49708938105, 1963.
- Uttal, T., Curry, J. A., McPhee, M. G., Perovich, D. K., Moritz, R. E., Maslanik, J. A., Guest, P. S., Stern, H. L., Moore, J.  
25 A., Turenne, R., Heiberg, A., Serreze, M. C., Wylie, D. P., Persson, O. G., Paulson, C. A., Halle, C., Morison, J. H., Wheeler, P. A., Makshtas, A., Welch, H., Shupe, M. D., Intrieri, J. M., Stamnes, K., Lindsey, R. W., Pinkel, R., Pegau, W. S., Stanton, T. P. and Grenfeld, T. C.: Surface Heat Budget of the Arctic Ocean, *Bull. Am. Meteorol. Soc.*, 83(2), 255–275, doi:10.1175/1520-0477(2002)083<0255:SHBOTA>2.3.CO;2, 2002.
- Vihma, T. and Pirazzini, R.: On the Factors Controlling the Snow Surface and 2-m Air Temperatures Over the Arctic Sea Ice  
30 in Winter, *Bound.-Layer Meteorol.*, 117(1), 73–90, doi:10.1007/s10546-004-5938-7, 2005.
- Vihma, T., Jaagus, J., Jakobson, E. and Palo, T.: Meteorological conditions in the Arctic Ocean in spring and summer 2007 as recorded on the drifting ice station Tara, *Geophys. Res. Lett.*, 35(18), doi:10.1029/2008GL034681, 2008.
- Walsh, J. E. and Chapman, W. L.: Arctic Cloud–Radiation–Temperature Associations in Observational Data and Atmospheric Reanalyses, *J. Clim.*, 11(11), 3030–3045, doi:10.1175/1520-0442(1998)011<3030:ACRTAI>2.0.CO;2, 1998.
- 35 Zhang, Y., Seidel, D. J., Golaz, J.-C., Deser, C. and Tomas, R. A.: Climatological Characteristics of Arctic and Antarctic Surface-Based Inversions, *J. Clim.*, 24(19), 5167–5186, doi:10.1175/2011JCLI4004.1, 2011.



Zygmuntowska, M., Mauritsen, T., Quaas, J. and Kaleschke, L.: Arctic Clouds and Surface Radiation – a critical comparison of satellite retrievals and the ERA-Interim reanalysis, *Atmospheric Chem. Phys.*, 12(14), 6667–6677, doi:10.5194/acp-12-6667-2012, 2012.